Received: 8 March 2019 | Revised: 23 July 2019 | Accepted: 24 August 2019

DOI: 10.1002/jrs.5743

RESEARCH ARTICLE

WILEY Journal of RAMAN SPECTROSCOPY

Discriminating polymorph distributions in pharmaceutical tablets using stimulated Raman scattering microscopy

Barbara Sarri[1] | Rafaël Canonge[1] | Xavier Audier[1] | Valérie Lavastre[2] | Géraldine Pénarier[2] | Jean Alie[2] | Hervé Rigneault[1]

[1] Aix Marseille Univ, CNRS, Centrale Marseille, Institut Fresnel, Marseille, France

[2] Sanofi Recherche & Développement, Sanofi, Montpellier, France

Correspondence
Hervé Rigneault, Institut Fresnel, Domaine Univ St Jérôme, 13397 Marseille CEDEX 20, France.
Email: herve.rigneault@fresnel.fr

Funding information
Agence Nationale de la Recherche, Grant/Award Numbers: 10-INSB-04-01, 11-IDEX- 0001-02 and 11-INSB-0006; Centre National de la Recherche Scientifique, Grant/Award Number: MI Raman Imaging

Abstract

Stimulated Raman scattering (SRS) imaging is used to probe active pharmaceutical ingredient exhibiting polymorphism within compact tablets. We show that few SRS images performed at selected wavenumbers allow to access both active pharmaceutical ingredients polymorphs and excipients from which molecular mapping is retrieved over millimetre-size areas. We exemplified the approach using SRS images acquired at five wavenumbers to map clopidogrel and amibegron polymorphs embedded into excipients (polyethylene glycol, corn starch, and mannitol tablets). Our study demonstrates that SRS imaging can be used as a novel fast molecular mapping technique for pharmaceutical tablets characterization.

KEYWORDS

active pharmaceutical ingredients (API), label-free imaging, molecular imaging, pharmaceutical tablets, polymorphism, stimulated Raman scattering (SRS)

1 | INTRODUCTION

The word polymorphism designates the ability of a compound to crystallize in more than one form.[1,2] Polymorphs are endowed with the same chemical composition but their packing (i.e., arrangement) and/or conformation differ.[3] This induces differences in their physicochemical properties and many parameters such as solubility, dissolution kinetic, thermodynamic stability, and bioavailability have been reported to be altered from one polymorph to another.[4] A well-known example is the antiretroviral ritonavir molecule, a medicine given in HIV treatment, whose efficiency dropped dramatically a few months after it was first launched on the market because the active drug had evolved into a more thermodynamically stable polymorph.[5] For the pharmaceutical industry, it is of crucial importance to control polymorphs synthesis and evolution in order to provide the more efficient form in medicines (i.e., the form that is more stable in time with the highest bioavailability as possible), and polymorph screening is nowadays a mandatory step when developing a new drug. More than 50% of all active pharmaceutical ingredients (API) are known to present polymorphic forms.[1,6] Therefore, monitoring potential phase transformations during tablet manufacturing process is very important, and different techniques are used[7] such as thermal analysis, differential scanning calorimetry (DSC), thermogravimetric analysis (TGA), X-ray powder diffraction (XRPD), solid-state nuclear magnetic resonance, and electron microscopy. Unlike TGA or DSC,[8] vibrational spectroscopy techniques such as infrared absorption and Raman scattering are interesting because they directly address the vibrational signature of molecular bonds present within a sample.[9] For instance, Raman spectroscopy is widely used in the pharmaceutical industry[10,11] because it is non-destructive, only a simple preparation is required and it enables to investigate polymorphism in amorphous materials, which is not the case when using XRPD.[3] However, spontaneous Raman spectroscopy suffers from a low cross section

that results in long acquisition times and makes molecular mapping time consuming.[12] Over the last decades, coherent Raman imaging techniques[13,14] such as coherent anti-Stokes Raman scattering (CARS) and stimulated Raman scattering (SRS) have emerged, taking advantage of the high ($\times 10^6$) enhancement due to the coherent addition of the vibrational emitters.[15] These techniques have spread over many fields to image cells,[16] tissues,[17,18] plants,[19] cosmetics,[20] nanoparticle drugs,[21] and pharmaceutical compounds.[22–27] However, only one study has been reported on polymorph imaging and identification using CARS.[28] In this paper, we use SRS to image and discriminate various polymorphs and excipients in pharmaceutical tablets over millimetre-size areas. Contrary to CARS,[29] SRS[30] is interesting because it scales linearly with concentration and is not affected by non-resonant background.[31] Here, we concentrate on two API: clopidogrel (Compound A) that is used to prevent platelet aggregations and reduces heart disease risks and strokes[32,33]; and amibegron (Compound B), an agonist targeting the beta-3 adrenergic receptor[34] that is used as antidepressant as well as anxiolytic due to its capability to enter the central nervous system.[35] For both compounds, two polymorphic forms F1 and F2 were studied. Measurements are presented for powders and compact tablets, including several excipients.

2 | MATERIAL AND METHODS

2.1 | Active pharmaceutical ingredients (API):

Clopidogrel (Compound A—Figure 1a) is known to have two polymorphic forms[36,37] denoted here A-F1 and A-F2. Amibegron (Compound B—Figure 1b) is also known to have two polymorphic forms denoted here B-F1 and B-F2.

Spontaneous Raman spectra of active compounds A and B were obtained on a commercial WITEC Raman spectrometer.

2.2 | Stimulated Raman microscopy

Stimulated Raman scattering imaging was performed on a custom-built set-up. A mode-lock Nd:YVO Laser (PicoTrain, HighQLaser) operating at 1,064 nm was on the one hand used as one of the optical sources and on the other hand, was frequency doubled to pump an optical parametric oscillator (OPO, Emerald, APE). Both Stokes (1,064 nm) and pump (OPO) beams consisted of picosecond pulse train (pulse duration 7 ps—~3 cm^{-1} SRS spectral resolution, repetition rate 80 MHz), which were recombined on the optical table and driven into a microscope (Nikon, TiU) to overlap both in space and time when arriving at the sample plane.[38] The pump beam was modulated at 20 MHz by an acousto-optics modulator (AA Optoelectronic MT200-AO) and was phase locked to the 80 MHz laser repetition rate thanks to ¼ frequency divider and phase shifter (APE, 137761). The stimulated Raman gain (SRG) signal was detected using a high speed photodiode and a fast lock-in amplifier (APE, LIA). During hyperspectral measurements, the OPO beam wavelength was tuned between 790 nm and 820 nm to address the full vibrational resonance region of the both API and excipients (2,800–3,200 cm^{-1}). Images acquisition was performed by means of point scanning using galvo mirrors (Cambridge Technology 6215H). The SRS signal could be detected both in the forward and in the epi-direction. Excitation and epi-collection were provided by an NA = 1.15 objective lens (Nikon APO LWD water 40×). A polarisation cube combined with a λ/4 waveplate allowed part of the back-reflected signal to be directed into the epi photodiode. In the forward direction, a condenser lens NA = 1.10 (Nikon APO LWD water 60×) was used to collect the light. In these conditions, the spatial resolution was 0.3 μm along the transverse directions (*x*-axis and *y*-axis) and 1 μm in the longitudinal direction (*z*-axis). Powers from each beam at the sample plane were 50 and 25 mW for tablets and powder, respectively. A custom-made Labview program[39] monitored the microscope stage movements allowing millimetre-size images to be acquired by stitching 100 μm × 100-μm images next to each other. Total time for a 100 μm × 100 μm SRS image was 8 s (dwell time per pixel 40 μs, 10 accumulations, pixel size 1 μm). In these conditions, a 1.1 mm × 1.1 mm stitched image required 25 min.

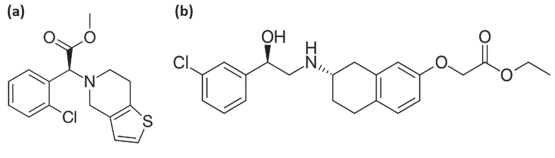

FIGURE 1 Active pharmaceutical ingredients. (a) Clopidogrel ($C_{16}H_{16}ClNO_2S$—321.819 g/mol—Compound A) and (b) amibegron ($C_{22}H_{26}ClNO_4$—403.903 g/mol—Compound B)

3 | RESULTS AND DISCUSSION

3.1 | Clopidogrel polymorph micro-crystals and mixture tablets

We concentrate first on Compound A (clopidogrel) and denote A-F1 and A-F2, the two polymorph forms. Figure 2a shows the spontaneous Raman spectra of polymorphs A-F1 and A-F2 crystals (size of few tens of

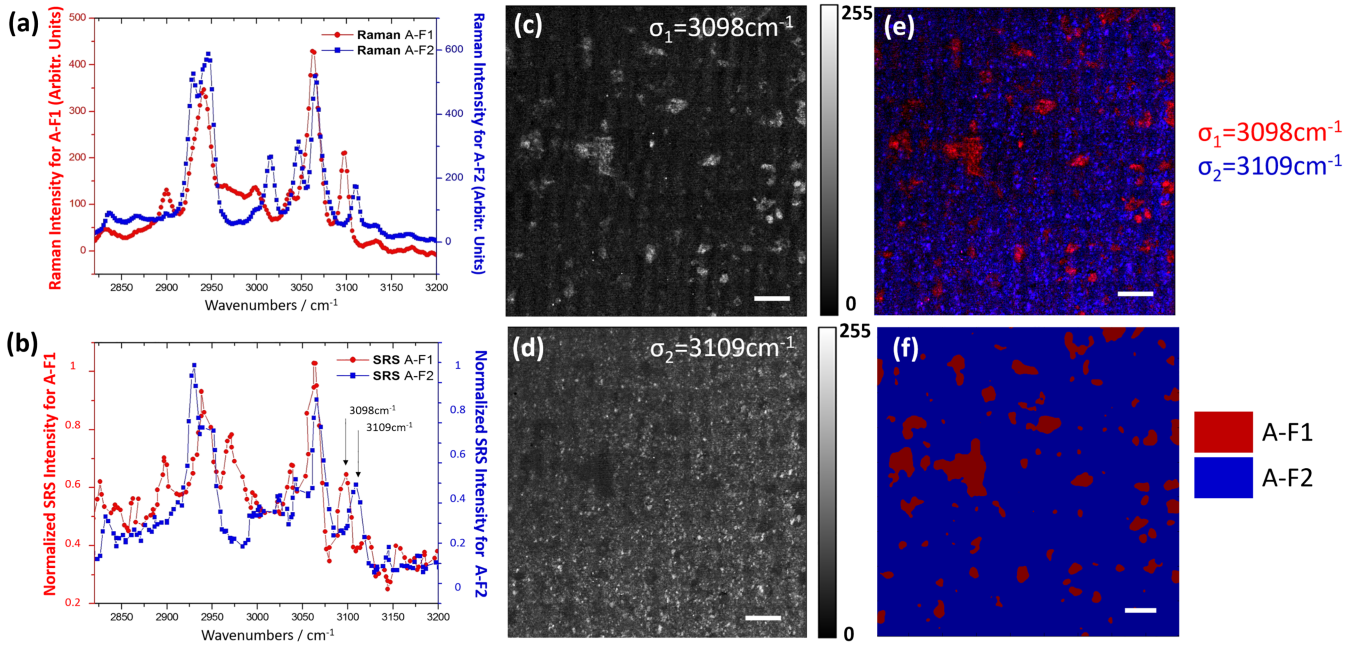

FIGURE 2 Discriminating polymorph active compounds in compact tablets using stimulated Raman scattering (SRS). (a) Raman spectra of species A-F1 (red) and A-F2 (blue) in the 2,800- to 3,200-cm^{-1} region. (b) SRS spectra of A-F1 (red) and A-F2 (blue) in the same region. Two wavenumbers, 3,098 and 3,109 cm^{-1}, are highlighted with arrows and are used for differentiating polymorphs A-F1 and A-F2, respectively. (c) A 1 × 1-mm backward-collected SRS image, at σ_1 = 3,098 cm^{-1}, of a tablet containing 90% of A-F2 and 10% of A-F1 (A-F1). (d) SRS image of the same area at σ_2 = 3,109 cm^{-1} (A-F2). (e) Merge picture of (c; red) and (d; blue). (f) Reconstruction binary map of species A-F1 (red) and A-F2 (blue). Scale bar is 100 μm

microns) between 2,800 and 3,200 cm^{-1}. Figure 2b shows the SRS spectra of the same crystals measured in transmission with a spectral step of 0.2 nm. Note that SRS spectra are obtained while tuning the OPO cavity wavelength that is subject to slight power variations across the explored spectrum range.

SRS spectra (Figure 2b) are found in fairly good agreement with the spontaneous Raman ones (Figure 2a) with all distinctive vibrational Raman bands visible. Performing hyperspectral SRS images stack between 2,800 and 3,200 cm^{-1} with our laser system is unpractical, as acquiring a spectrum over this frequency range (Figure 2b) takes 45 min due to the relatively slow OPO cavity temperature tuning. To overcome this time constrain, we concentrate on two high-frequency wavenumbers, σ_1 = 3,098 cm^{-1} and σ_2 = 3,109 cm^{-1}, to identify A-F1 and A-F2, respectively (Figure 2b). These two wavenumbers are close enough to allow fast (few hundreds of millisecond) OPO cavity tuning using the OPO Lyot filter only and without readjusting the temperature of the OPO crystal. Subsequently, tablets solely composed of the two polymorphs (A-F1:A-F2 ratio equal to 10:90) were imaged over 1 mm × 1 mm at wavenumbers σ_1 and σ_2 with the SRS signal recorded in epi-direction (Figure 2c,d). When overlaid, the two polymorphs appear with a complementary distribution (Figure 2e) where pure A-F1 large crystal patches are immersed into A-F2 granules. This distribution allows a binary display (present/absent) of this A-F1:A-F2 mixture as shown in Figure 2f (red: Compound A-F1, blue Compound A-F2). This demonstrates the capability of SRS for discriminating between the two polymorphs of interest.

3.2 | Clopidogrel polymorph tablet containing excipients

In pharmaceutical tablets, the API generally represents a minor portion of the ingredient volume. Other ingredients are usually functional excipients ensuring tablet integrity, taste, conservation of the API, and other aspects. Excipients must be safe and chemically compatible with the API. Excipients are also used to preserve, protect or stabilize the API until it arrives to its targeted destination, facilitate or control API release, and optimize its bioavailability. Excipients are classified into different families amongst which organic molecules (starch, sugars, and cellulose) represents more than 90%[40]. To mimic real pharmaceutical tablet, we have selected mannitol, polyethylene glycol (PEG), and corn starch as being three common excipients. Mannitol is commonly used as a diluent (i.e., a species that will fill the tablet volume) due to its good secondary properties: It eases the

compression and it can, in addition, be used as a sweetening agent.[41] PEG is often used as a plasticizer, a solvent or a lubricant in tablet and capsules during oral dosage from manufacturing processes. Sometimes, it can also be used as a thickening agent or a binder: An agent that helps particles to link together; binders are mainly used to decrease the pressure during tablet manufacturing.[42] Starch is a multiple-task excipient, which is used as a binder, a diluent, and a disintegrant agent (once mixed with the solvent, it facilitates the tablet dissolution[42]).

Tablets fabricated for this study have specific excipient ratios so that starch: PEG6000: mannitol was 80:10:10. Polymorphic form concentrations were also monitored to reach 20:80 for A-F1:A-F2. APIs to excipients ratio was 50:50 so that the final composition of the tablet was A-F1 10%, A-F2 40%, mannitol 5%, PEG6000 5%, and starch 40%. To guarantee the ability of SRS to distinguish between the various ingredients, a preliminary hyperspectral study was performed, directly on the tablet (Figure 3e). SRS images were acquired using the same

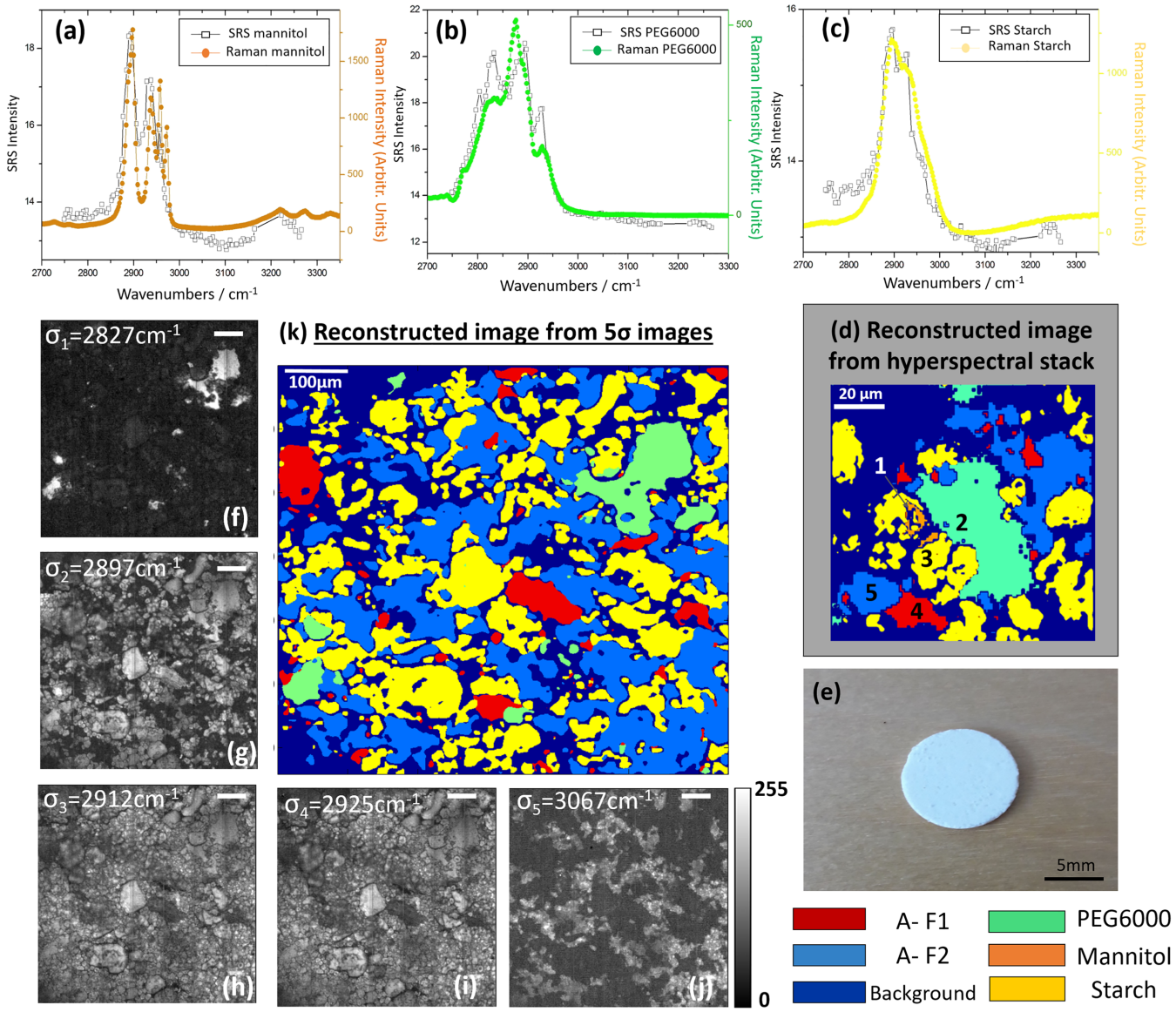

FIGURE 3 Discriminating cClopidrogrel polymorphs A-F1 and A-F2 from excipients in pharmaceutical tablets using SRS imaging. (a–c) SRS (black empty squares) and Raman (colour-ed filled dots) spectra over the 2,700–3,300 cm^{-1} region: spectra of (a) mannitol, (b) PEG600, and (c) starch corn. (d) Reconstruction map of the different elements present within the tablet using a 100 µm × 100 µm hyperspectral SRS image. (e) Picture of the tablet imaged. (f–j) SRS images of a 650 µm × 650 µm area of the tablet at different wavenumbers allowing to extract the distribution of each of the three excipients, and of the two polymorph forms A-F1 and A-F2. SRS signal distribution at: (f) σ_1 = 2,827 cm^{-1}, (g) σ_2 = 2,897 cm^{-1}, (h) σ_3 = 2,912 cm^{-1}, (i) σ_4 = 2,925 cm^{-1}, and (j) σ_5 = 3,067 cm^{-1}. (k) Reconstruction map of the different elements present in the 650 µm × 650 µm wavenumbers recorded in (f–j): A-F1 (red), A-F2 (light blue), PEG6000 (green), mannitol (orange), and starch (yellow). The background appears in dark blue. Scale bar is 100 µm

conditions as before (one image every 0.3 nm in the extended lipid region [2,800–3,200 cm^{-1}], detection in the epi-direction). Very distinct image patterns were disclosed with respect to increasing wavenumbers (Figure 3f,j). Perfect complementarity of the patterns at pinpointed wavenumbers substantiated that ingredients, neither APIs nor excipients, did not spatially overlap (Figure 3d). SRS spectra of three region of interest (ROI), highlighted with numbers 1–3 in Figure 3d, were juxtaposed to the spontaneous Raman spectra of the excipients. Results are presented in Figure 3a,c: Spectral characteristics of each excipient could be retrieved without difficulty. SRS spectra show a satisfactory match with the spontaneous Raman spectra profiles (see discussion below) of mannitol (Figure 3a), PEG6000 (Figure 3b), and starch (Figure 3c). This allowed assigning ROI 1–3 to mannitol, PEG, and starch, respectively. Remaining patterns were identified as the two polymorphs A-F1, A-F2: Spectra of ROI 4 and 5 were similar to the ones shown in Figure 2b.

3.3 | Decision tree approach for polymorphs and excipients sorting

A restricted number of images acquired at different wavenumbers, showing the highest spatial diversity, were manually chosen from the hyperspectral stack to feed a simple decision tree algorithm that identifies ingredients at each pixel of the image. The algorithm relies on the exclusive hypothesis that a unique component is present per pixel. This assumption is both supported by the distinct image patterns observed at different wavenumbers and the fact that components are solids separated into mesoscopic domains in the crystalline or amorphous states. First, a threshold is applied on each of the five selected wavenumber (σ_1, σ_2, σ_3, σ_4, σ_5) images in order to extract useful information from the background noise. Data at selected wavenumber (σ_1, σ_2, σ_3, σ_4, σ_5) are considered as five equations with five unknown variables (*A-F1, A-F2, excip$_1$, excip$_2$,* and *excip$_3$*) where *excip$_1$* is starch, *excip$_2$* PEG6000, and *excip$_3$* mannitol. Component allocation for each pixel is performed sequentially following that if the value of a pixel of coordinates (i,j), at wavenumber σ_n (i,j), is above the threshold and is not already assigned to a previous component in the chain, the pixel is allocated to the new component. For Compound A (clopidogrel), the algorithm used (2,827, 2,897, 2,912, 2,928, and 3,067 cm^{-1}) for σ_1, σ_2, σ_3, σ_4, and σ_5 (Figure 3f,j) and the decision tree allocations is as follows:

$$\sigma_5(\mathrm{i},\ \mathrm{j}): A - F2 \rightarrow \boldsymbol{A\text{-}F2}, \quad (1)$$

$$\sigma_1(\mathrm{i},\ \mathrm{j}): excip_2 \rightarrow \boldsymbol{excip_2}, \quad (2)$$

$$\sigma_3(i,\ j): A - F2,\ excip_1,\ excip_2 \rightarrow \boldsymbol{excip_1}, \quad (3)$$

$$\sigma_4(i,\ j): A - F2,\ excip_1,\ excip_2,\ excip_3 \rightarrow \boldsymbol{excip_3}, \quad (4)$$

$$\sigma_2(\mathrm{i},\ \mathrm{j}): A - F1,\ excip_1,\ excip_2,\ excip_3 \rightarrow \boldsymbol{A\text{-}F1}. \quad (5)$$

Presence/absence of the components at the chosen pinpointed wavenumbers was known from the SRS spectra profiles. Element distributions were then de-noised using comparisons with the first four and eight neighbours. Gaussian blur was applied to smooth the patterns and get a binary map (present/absent) for each ingredient. To obtain the final map, binary maps were summed using different coefficients; priority conditions were applied to avoid eventual overlaps between the species due to the smoothing. Figure 3d shows the results of the algorithm using only images (σ_1, σ_2, σ_3, σ_4, σ_5) of the 100 × 100 μm hyperspectral stack.

The proposed "5σ" decision tree algorithm benefits from its straightforward implementation as it is requiring only five SRS images at selected wavenumber (σ_1, σ_2, σ_3, σ_4, σ_5); it nonetheless requires to be initialized to set appropriate thresholds and choose relevant wavenumbers for each species. A preliminary Raman or SRS spectral study is mandatory and can be performed on a small region of a sample involving the unknown components. Nevertheless, once initialized, for a set of molecular species, wavenumbers and thresholds can be reused to explore other samples containing a subset of known compounds or larger regions within reduced time. This is illustrated in Figure 3f,j where a 0.5 mm area was probed at selected wavenumber (σ_1, σ_2, σ_3, σ_4, σ_5) exclusively (100 points per 100 μm × 100 μm, 40 μs per pixel, 10 accumulations) requiring a data acquisition time of 10 min per wavenumber to scrutinize the 0.7 mm × 0.7 mm region. With this, it took less than 1 h to get the entire set of data to map the various polymorphs and excipients in this area. This is to compare to the 12 h that is usually necessary to map the components of such a tablet over the same area using spontaneous Raman. Here, to compensate for the roughness of the tablet surface, three different z planes, 5 μm apart from each other, were probed and summed for each wavenumbers before analysis with the algorithm. Figure 3f,j shows the SRS data recorded at the selected wavenumbers (σ_1, σ_2, σ_3, σ_4, σ_5), and the results of the proposed decision tree approach is shown in Figure 3k. Note that the areas referred as "background" are actually filled with air and reflect the intersection between the SRS-sectioned imaged planes and the very rough surface of the imaged tablet. PEG domains are

easily recognizable in Figure 3f as it is the only specie showing strong vibrational signatures at lower wavenumbers (PEG is rich in CH_2). These PEG domains show no distinguishable crystalline structures and are very variable in size (few microns up to hundreds of microns). Starch characteristic structural shape could be visualized on Figure 3g,h. This excipient exhibiting a strong chemical signature over the whole 2,900–2,930 cm^{-1} spectral region. Starch domains are mostly composed of 20 μm spherical granules dispersed in groups quite homogeneously distributed over the surface, with the presence of some larger disparate elements also uniformly spaced. This peculiar probed region is found exempted from mannitol (Figure 3k). Excipients manifest higher signals compared with the API. Remarkably, wavenumbers used to discriminate the polymorphs in this mixture were quite different from the wavenumbers preselected with the pure powders (Figure 2). Polymorph A-F1 manifested a weak signature at high wavenumbers compared with A-F2 and its signal was hardly detectable around 3,100 cm^{-1} (data not shown). This species exhibited some vibrational resonance only around 2,897 cm^{-1} (see Figure 3g) and could only be discriminated at last in the decision tree. As for A-F_2, the vibrational signature at 3,067 cm^{-1} showed a better SNR than 3,110 cm^{-}1, and the SRS signal at this wavenumber provided directly the polymorph distribution because excipient signals were quasi-inexistent at such a high wavenumber (Figure 2j). Hence and unexpectedly, the couple (2,897 cm^{-1}, 3,070 cm^{-1}) proved to be a far more suitable wavenumber pair to detect the A-F1 and A-F2 polymorph signatures when associated with the excipients. After exclusion of the pixels allocated to the background, the composition of the tablet for the region imaged could be retrieved from the final map reconstruction (Figure 3k) and provided: A-F1 7%, A-F2 43%, mannitol 0%, PEG6000 7.5%, and starch 42.5%. It could therefore be concluded that the final APIs and excipient ratios were in fairly good agreement with the manufactured preparation composition; the only major difference is the lack of mannitol in the imaged region; possibly due to the non-perfect homogeneity of the mixture of excipients. Nevertheless, the 50:50 APIs/excipient ratio was respected.

3.4 | Amibegron (Compound B) polymorph tablet containing excipients

Experiments were repeated using amibegron as the second API (Compound B) whose spontaneous Raman spectra for the two polymorphic forms, B-F1 and B-F2, are given in Figure 4g, in red and blue, respectively. Like for Compound A, crystal powder of pure polymorph species were probed spectrally with SRS (forward detection). Here again, SRS spectral features of both B-F1 and B-F2 showed fairly good agreements with the spontaneous Raman data (Figure 4h).

Tablets mixing B-F1 and B-F2 with the three excipients (PEG, starch, and mannitol) were investigated. In this case, B-F_1: B-F_2 ratio was 10:90 whereas excipients ratio remained 80:10:10 for starch: PEG6000: mannitol. APIs to excipients ratio was 20:80 to further mimic real pharmaceutical conditions so that the final composition of this tablet was: B-F1 18%, B-F2 2%, mannitol 8%, PEG6000 8%, and starch 64%. SRS images from the tablet were acquired in the epi-direction and with the same conditions as for Compound A, for both SRS hyperspectral imaging and images acquisition at pinpointed wavenumbers. The only exception arose from the size of the region probed: This time, a 1.1 × 1.1-mm large region was explored at a unique z plan (compared with the three z-plan probed for Compound A).

Again, a preliminary hyperspectral study was performed to pinpoint appropriate wavenumbers. Determination of suitable vibrational bands for the new set of API also took advantage of the presence of distinct vibrational modes for B-F1 and B-F2 at higher wavenumbers, in the 2,975–3,130 cm^{-1} region, where excipient spectral signatures are extremely weak. Unlike previously, in this case, both polymorph distributions could be retrieved quasi-instantaneously (providing thresholding) in pharmaceutical tablets containing both polymorphs and the three excipients: This was performed using the wavenumbers 3,055 and 2,974 cm^{-1} to detect B-F1 and B-F2, respectively. As before, PEG distribution was collected targeting the CH_2 vibrational band at 2,840 cm^{-1} whereas starch and mannitol distributions could be retrieved from the SRS data at 2,905 and 2,930 cm^{-1}, respectively.

The following wavenumbers were selected for the algorithm: 2,841, 2,905, 2,931, 2,974, and 3,053 cm^{-1} for (σ_1, σ_2, σ_3, σ_4, σ_5), and the decision tree for component allocations follows:

$$\sigma_5(\mathrm{i},\ \mathrm{j}): B-F1 \rightarrow \boldsymbol{B\text{-}F1}, \quad (1)$$

$$\sigma_1(\mathrm{i},\ \mathrm{j}): excip_2 \rightarrow \boldsymbol{excip_2}, \quad (2)$$

$$\sigma_4(\mathrm{i},\ \mathrm{j}): B-F2 \rightarrow \boldsymbol{B\text{-}F2}, \quad (3)$$

$$\sigma_2(\mathrm{i},\ \mathrm{j}): B-F2,\ excip_1,\ excip_2 \rightarrow \boldsymbol{excip_1}, \quad (4)$$

$$\sigma_3(i,\ j): B-F1,\ B-F2, excip_1,\ excip_2,\ excip_3 \rightarrow \boldsymbol{excip_3}. \quad (5)$$

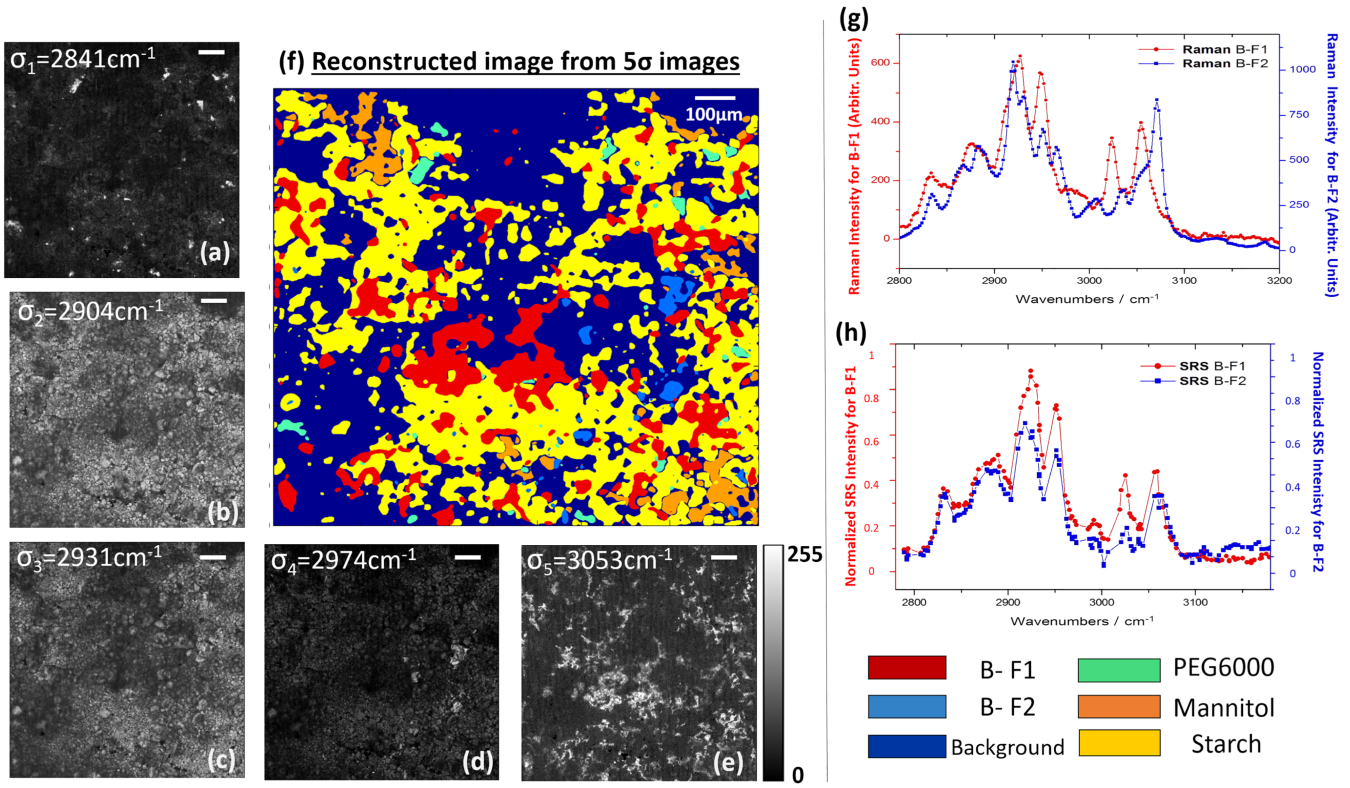

FIGURE 4 Discriminating amibegron polymorphs B-F1 and B-F2 from excipients in pharmaceutical tablets using SRS imaging. (a–e) 1.1 mm × 1.1-mm SRS images of a tablet at different wavenumbers allowing to extract the distribution of three excipients and two polymorphs, B-F1 and B-F2. SRS signal distribution at (a) σ_1 = 2,841 cm^{-1}, (b) σ_2 = 2,904 cm^{-1}, (c) σ_3 = 2,931 cm^{-1}, (d) σ_4 = 2,974 cm^{-1}, and (e) σ_5 = 3,053 cm^{-1}. (f) Reconstruction map of the different elements present within the area are the following: B-F1 (red), B-F2 (light blue), PEG (green), mannitol (orange), and starch (yellow). The background appears in dark blue. Scale bar is 100 µm. (g) Raman spectra of the two amibegron polymorphs, B-F1 (red) and B-F2 (blue), in the 2,800- to 3,200-cm¯1 region, (h) SRS spectra of B-F1 (red) and B-F2 (blue) over the same region

Figure 4a–e summarizes the SRS data whereas Figure 4f displays the reconstructed map deduced from the "5σ" decision tree approach. Starch distribution was similar to when mixed with Compound A whereas only smaller domains (smaller than 50 µm) could be seen for PEG. Here, mannitol domains could be observed (orange domains in Figure 4f), this species seemed to interact with starch mainly. As for the case of clopidogrel tablet containing excipients, large dark blue zones entitled "background", arose from the roughness of the tablet, the surface in these regions being situated a few microns below the acquisition plan. Ingredient ratios from Figure 4f also proved to be fairly concordant with the tablet preparation: B-F1 22%, B-F2 2%, mannitol 6.5%, PEG6000 2%, and starch 66.5% against B-F1 18%, B-F2 2%, mannitol 8%, PEG6000 8%, and starch 64% given by the manufacturer for the tablet composition.

We note a satisfactory agreement between the spontaneous Raman and SRS spectra (Figures 2a,b, 3a,b,c, and 4g,h) although some marked differences remain. We attribute these differences to several factors. First, the SRS spectral resolution was of the order of ~3 cm^{-1}, which is worse than the one achieved with the spontaneous Raman spectrometer ~1 cm^{-1}. Second, the SRS polarized backward detection is sensitive to the Raman depolarization ratio of the probed Raman lines that may affect their relative intensities. Third, although the spontaneous Raman spectrometer used a non-polarized laser and that the SRS polarization states of the incoming pump and Stokes beam were circular, we cannot rule out that the crystalline nature of the pharmaceutical ingredient brought some anisotropy.

4 | CONCLUSION

In this study, SRS microscopy was used to visualize pharmaceutical tablet compositions in a time scale that is ×20 faster than spontaneous Raman mapping. We have shown that SRS was suitable to image various ingredients with sub-micron resolution and minute spectral variation (11 cm^{-1} in the case of A-F1 and A-F2). Using

hyperspectral imaging, we were able to pinpoint a few wavenumbers of interest and could highlight API (clopidogrel and amibegron) polymorph signatures from the excipients (PEG, starch, and mannitol) they were mixed with. Molecular distribution could be retrieved for each species using five wavenumbers together with a dedicated decision tree algorithm. For the pharmaceutical industry, it is of utmost importance to control polymorphism because physicochemical properties are altered in case of polymorph transformation, and polymorphic changes can be dramatic for API bioavailability. We have demonstrated that SRS imaging could be used as a novel fast molecular mapping technique for pharmaceutical tablets characterization over millimetre-size areas. Alternatively, SRS could also be a useful tool to probe polymorphic stability over time or in the presence of water during tablet dissolution.

ACKNOWLEDGEMENTS

The authors acknowledge financial support the Centre National de la Recherche Scientifique (MI Raman Imaging), Aix-Marseille University A*Midex (noANR-11-IDEX- 0001-02), and Agence Nationale de la Recherche grants France Bio Imaging (ANR-10-INSB-04-01) and France Life Imaging (ANR-11-INSB-0006) infrastructure networks.

CONFLICT OF INTEREST

The authors state no conflict of interest.

ORCID

Hervé Rigneault https://orcid.org/0000-0001-6007-0631

REFERENCES:

[1] S. A. Kaisar Raza, P. Kumar, S. Ratan, R. Malik, *SOJ Pharm Pharm Sci* **2014**, *1*, 10.

[2] N. L. Prasanthi, M. Sudhir, N. Jyothi, and V. Sri, "A review on polymorphism perpetuates pharmaceuticals," **2016**.

[3] E. H. Lee, *Asian J Pharm Sci* **2014**, *9*, 163.

[4] J. Haleblian, W. McCrone, *J Pharm Sci* **1969**, *58*, 911.

[5] J. F. Bauer, *J Valid Technol* **2008**, 15.

[6] B. P. H. Karpinski, Polymorphism of active pharmaceutical ingredients, **2006**, 2, 233.

[7] H. Li, Y. Kiang, J. Jona, *Eur J Pharm Sci* **2009**, *38*, 426.

[8] P. Patnaik, *Dean's Anal Chem Handb*, p. electronic copy **2004**.

[9] B. Schrader, *Infrared and Raman Spectroscopy*, VCH Publishers Inc **1995**.

[10] S. Cînta Pinzaru, I. Pavel, N. Leopold, W. Kiefer, *J Raman Spectrosc* **2004**, *35*, 338.

[11] A. P. Ayala, *Vib Spectrosc* **2007**, *45*, 112.

[12] S. Wartewig, R. H. H. Neubert, *Adv Drug Deliv Rev* **2005**, *57*, 1144.

[13] W. Min, C. W. Freudiger, S. Lu, X. S. Xie, *Annu Rev Phys Chem* **2011**, *62*, 507.

[14] J.-X. Cheng, X. S. Xie, *Science* **2015**, *350*, 6264.

[15] H. Rigneault, P. Berto, *APL Photonics* **2018**, *3*, 091101.

[16] T. Minamikawa, H. Niioka, T. Araki, M. Hashimoto, *J Biomed Opt* **2011**, *16*, 2.

[17] P. Gasecka, A. Jaouen, F.-Z. Bioud, H. B. de Aguiar, J. Duboisset, P. Ferrand, H. Rigneault, N. K. Balla, F. Debarbieux, S. Brasselet, *Biophys J* **2018**, *113*, 1520.

[18] M. Ji, S. Lewis, S. Camelo-Piragua, S. H. Ramkissoon, M. Snuderl, S. Venneti, A. Fisher-Hubbard, M. Garrard, D. Fu, A. C. Wang, J. A. Heth, C. O. Maher, N. Sanai, T. D. Johnson, C. W. Freudiger, O. Sagher, X. S. Xie, D. A. Orringer, *Sci Transl Med* **2015**, *7*, 309.

[19] J. C. Mansfield, G. R. Littlejohn, M. P. Seymour, R. J. Lind, S. Perfect, J. Moger, *Anal Chem* **2013**, *85*, 5055.

[20] X. Chen, S. Grégoire, F. Formanek, J. B. Galey, H. Rigneault, *J Control Release* **2015**, *200*, 78.

[21] N. Garrett, A. Lalatsa, D. Begley, L. Mihoreanu, I. F. Uchegbu, A. G. Schatzlein, J. Moger, *J Raman Spectrosc* **2012**, *43*, 681.

[22] M. N. Slipchenko, H. Chen, D. R. Ely, Y. Jung, M. T. Carvajal, J.-X. Cheng, *Analyst* **2010**, *135*, 2613.

[23] E. T. Garbacik, J. L. Herek, C. Otto, H. L. Offerhaus, *J Raman Spectrosc* **2012**, *43*, 681.

[24] M. Jurna, M. Windbergs, C. J. Strachan, L. Hartsuiker, C. Otto, P. Kleinebudde, J. L. Herek, H. L. Offerhaus, *Journal of Innovative Optical Health Sciences* **2009**, *2*, 37.

[25] D. Novakovic, J. Saarinen, T. Rojalin, O. Antikainen, S. J. Fraser-Miller, T. Laaksonen, L. Peltonen, A. Isomaki, C. J. Strachan, *Anal Chem* **2017**, *89*, 11460.

[26] M. Windbergs, M. Jurna, H. L. Offerhaus, J. L. Herek, P. Kleinebudde, C. J. Strachan, *Anal Chem* **2009**, *81*, 2085.

[27] A. L. Fussell, P. Kleinebudde, J. Herek, C. J. Strachan, H. L. Offerhaus, *J Vis Exp* **2014**, *89*, 1.

[28] E. T. Garbacik, A. L. Fussell, S. Gures, J. P. Korterik, C. Otto, J. L. Herek, H. L. Offerhaus, in *In Multiphoton Microscopy in the Biomedical Sciences Xiii*, (Eds: A. Periasamy, K. Konig, S. Ptc) Vol. 8588 **2013**.

[29] A. Zumbusch, G. R. Holtom, X. S. Xie, *Phys Rev Lett* **1999**, *82*, 4014.

[30] C. W. Freudiger, W. Min, B. G. Saar, S. Lu, G. R. Holtom, C. W. He, J. C. Tsai, J. X. Kang, X. S. Xie, *Science* **2008**, *322*, 1857.

[31] H. Rigneault, D. Gachet, in *in* Raman Imaging: Techniques and Applications, (Ed: A. Zoubir), Springer, Berlin Heidelberg **2012** 347.

[32] M. J. Price, J. S. Walder, B. A. Baker, D. E. Heiselman, J. A. Jakubowski, D. K. Logan, K. J. Winters, W. Li, D. J. Angiolillo, *J Am Coll Cardiol* **2012**, *59*, 2339.

[33] E. R. Bates, W. C. Lau, D. J. Angiolillo, *J Am Coll Cardiol* **2011**, *57*, 1251.

[34] J. Stemmelin, C. Cohen, J.-P. Terranova, M. Lopez-Grancha, P. Pichat, O. Bergis, M. Decobert, V. Santucci, D. Françon, R. Alonso, S. M. Stahl, P. Keane, P. Avenet, B. Scatton, G. le Fur, G. Griebel, *Neuropsychopharmacology* **2008**, *33*, 574.

[35] D. H. Overstreet, J. Stemmelin, G. Griebel, *Pharmacol Biochem Behav* **2008**, *89*, 623.

[36] H.-J. Kim, K.-J. Kim, *Ind Eng Chem Res* **2009**, *48*, 11133.

[37] J. Lu, L. W. Chen, J. Wang, Z. Li, *Asian Journal of Chemistry* **2013**, *25*, 1999.

[38] S. Brustlein, P. Ferrand, N. Walther, S. Brasselet, C. Billaudeau, D. Marguet, H. Rigneault, *J Biomed Opt* **2011**, *16*, 21106.

[39] P. Ferrand, *Comput Phys Commun* **2015**, *192*, 342.

[40] A. Katdare, *Excipient Development for Pharmaceutical, Biotechnology, and Drug Delivery Systems*. **2006**.

[41] Rowe, *Handb Pharm Excipients* **2012**, 479.

[42] P. J. S. and S. C. O. Raymond C Rowe, *Handbook of Pharmaceutical Excipient, 5th edition*. **2016**.

How to cite this article: Sarri B, Canonge R, Audier X, et al. Discriminating polymorph distributions in pharmaceutical tablets using stimulated Raman scattering microscopy. *J Raman Spectrosc*. 2019. https://doi.org/10.1002/jrs.5743